TELKOMNIKA Telecommunication Computing Electronics and Control
Vol. 20, No. 2, April 2022, pp. 383~391
ISSN: 1693-6930, DOI: 10.12928/TELKOMNIKA.v20i2.22462

The detection of oil spill onshore using the thermal band of landsat-8

Dheya Uldeen K. Abbas[1], Loay E. George[2]
[1]Department of Physics, College of Science, University of Baghdad, Iraq
[2]University of Information Technology and Communication, Baghdad, Iraq

Article Info

Article history:

Received Apr 13, 2021
Revised Feb 07, 2022
Accepted Feb 15, 2022

Keywords:

Interpolation
Landat-8
NDVI
Oil spill
Thermal radiation

ABSTRACT

Remote sensing is an advanced technique that can be used to detect hydrocarbons on land, and its advantages include rapid and low-cost detection. The detection of hydrocarbons on the surface is essential for environmental monitoring and the purpose of exploration. For oil and gas companies, the ability to locate hydrocarbon spill sites is important information for the success of future exploration wells. This study aimed to determine the quantities of hydrocarbons mixed with the soil as an indicator of its accumulation in the subsurface. In this paper, temperature data obtained from the landsat-8 satellite were used to determine the extent of the oil spill in the area using spatial interpolation and gradient techniques. Kriging interpolation is based on statistical models (i.e. including auto-correlation) geostatistical techniques can produce a forecast surface and also provide accurate forecasts. The results showed that there are 60 sites of thermal anomalies and temperature values are lowest and highest 23.2 ºC to 91.11 ºC, in the study area. Three different sites were chosen in terms of area and effect. They are located in the northern and southern Rumaila and Zubair fields. The location of the oil spills was determined with high accuracy after identifying the anomalies.

Corresponding Author:

Dheya Uldeen K. Abbas
Department of Physics, College of Science, University of Baghdad
Baghdad, Iraq
Email: dhiaa.khdeer1204@sc.uobaghdad.edu.iq

1. INTRODUCTION

Hydrocarbon seepage systems are natural phenomena that occur when the hydrocarbon traps are not completely sealed. In such a case the hydrocarbons may escape from the subsurface source situated either offshore or onshore to the surface. It is estimated that about 75% of the world's oil basins show hydrocarbon spills [1], [2]. In the onshore domain, the aspects of oil and gas seepage can be divided into two categories: a) macroseepage and b) microseepage. Macroseepages correspond to the accumulation of hydrocarbons (HCs) on the surface directly visible by the naked eye whereas microseepages are defined as traces of invisible light HCs in soils and which are only detectable by analytical methods.

Hydrocarbon spills are a global problem, which can have a negative impact on human life and the environment. Therefore, early identification and taking necessary remedial measures are essential [3]. The hydrocarbons that appear on the surface cause oxidation and reduction reactions at sites or along migration paths. As a result, sediment and water anomalies occur [4]. In close-surface sediments, mineralogical changes and changes in electrical, magnetic and seismic property are observed [5]. Hydrocarbon pollution can affect vegetation and cause changes in vegetation (bio) physical parameters (pigments, water, and content), depending on the species, pollutant type, and exposition period [6].

The hydrocarbon absorbs part of the solar radiation and emits it in the region 8 μm and 14 μm of the spectrum, as thermal energy. In infrared (IR) images on the basis of physics, every object with a temperature greater than absolute zero emits energy in the form of electromagnetic radiation [7], [8]. A black body is a hypothetical or model body that absorbs all the radiation falling on it and does not reflect or transmit it. It's a perfect radiation emitter and a perfect absorber over all wavelengths. It takes values without dimensions ranging from (0 to 1) [9]. The thermal energy emitted from the black body is distributed spectrally depending on its temperature only. This radiation is referred to as thermal radiation. However, the amount of thermal radiation freed depends on the emitted surface of the body for any particular temperature and wavelength [10].

Remote sensing plays an important role in detecting oil spill response efforts to measure oil spills in large fields are often difficult because they require a very expensive and time-consuming processes such as inspecting large affected areas, affected area monitoring, and other field measurements. While remote sensing by satellite can provide information easily and effectively in large areas and at a lower cost [11]. One of the satellite sensors, landsat 8, was successfully launched in 2013 by National Aeronautics and Space Administration (NASA) and the United State Geological Survey (USGS); it is a ground-monitoring satellite that covers the same area once every 16 days. A scene of a landsat 8 image generally covers an area of 185×185 km^2. It is equipped with two sensors: the operational land imager (OLI) and the thermal infrared sensor (TIRS). OLI gathers data with a 30 m spatial resolution with eight bands situated in the visible, near-infrared, and shortwave infrared portions of the electromagnetic spectrum, as well as a 15 m panchromatic band. TIR radiance is measured at a spatial resolution of 100 m by TIRS, which employs two thermal bands situated in the atmospheric window between 10 and 12 μm for continuous earth observations to provide for the estimation of land surface temperature (LST) [12], [13]. The landsat-8 satellite using both thermal image channels (i.e. 10 and 11) to provided temperature data. Band 10 was used to retrieve the Earth's surface temperature using the algorithm described in the work steps.

This study aimed to determine the quantities of hydrocarbons mixed with the soil as an indicator of its accumulation in the subsurface. Using a unique method for surveying and exploring an area of interest. This project aims to use remote sensing to detect the thickness of oil spills at different regions surrounding the oil fields. Various infrared bands will be examined to assess the accuracy of using them for determining the spill regions. And select the quantities of hydrocarbons mixed with the soil as an indicator of its accumulation in the subsurface. Using digital processing techniques for satellite visuals and Google images to deduce and identify surface evidence of oil spills. Detection of oil spills by remote sensing is a very important topic and many papers have been published in this field [14]. Such as radar images are able to operate at night or day and with clouds or fog. They can be used to detect oil spills in water, but they are limited to some monitoring conditions and have many limitations [15]. Also, the laser fluorosenseor is the most commonly utilized device. Due to its unique capacity to recognize oil on backdrops which include soil, water, ice and snow. The drawbacks are big size, weight and expensive cost [16].

2. RESEARCH METHOD

The research area in this case study is located in southern Iraq between longitudes (48°30´E-46° 40´E) and latitude (31° 20´ N-29° 50´ N). This governorate is considered one of the important governorates in Iraq, as it is rich in oil fields. These include the Rumaila field, the Shaiba fields, the West Qurna field, and the Majnoon fields. This region has a high concentration of hydrocarbon (HC), particularly as an oil and gas producer.The occurrence of shale gas and HC seepage in this region indicates that HC is very potent. The study area is shown in Figure 1.

2.1. Materials and methods

In this study, landsat-8 data were used to estimate the land surface temperature based on thermal band 10 to calculate the brightness temperature and infrared band 5 and red band 4 to calculate normalized difference vegetation index (NDVI) of the study area. Knowing the NDVI value is essential to determine proportional vegetation and emissivity. The land surface temperature can be derived from these bands.

2.2. The used data

Landsat 8 is a United States ground-monitoring satellite (USGS) that covers the same area once every 16 days. Its data can be obtained free on the website of the USGS. Satellite imagery data were used for Al-Basrah region in October of 2020. The image was already rectified to WGS-1984-UTM-Zone_38N.

2.3. The software's used

– ArcGIS 10.7: it is an advanced integrated system in geographic information systems, and it is produced by the American company environmental systems research institute (ESRI). ArcMap enables users to

view, modify, produce, and analyze geospatial data. This program is used for the final output of satellite images.

- Surfer 16: surfer is a contouring and 3D surface mapping software program that runs under Microsoft Windows. The Surfer software quickly and easily converts data into outstanding contour, surface, wireframe, vector, image, shaded relief, and post maps. This program is used for the Interpolation map.
- Matlab R2019b: Matlab allows matrix manipulations, plotting of functions and data, implementation of algorithms, creation of user interfaces, and interfacing with programs written in other languages. This program was used to solve a gradient equation and draw a map of it.

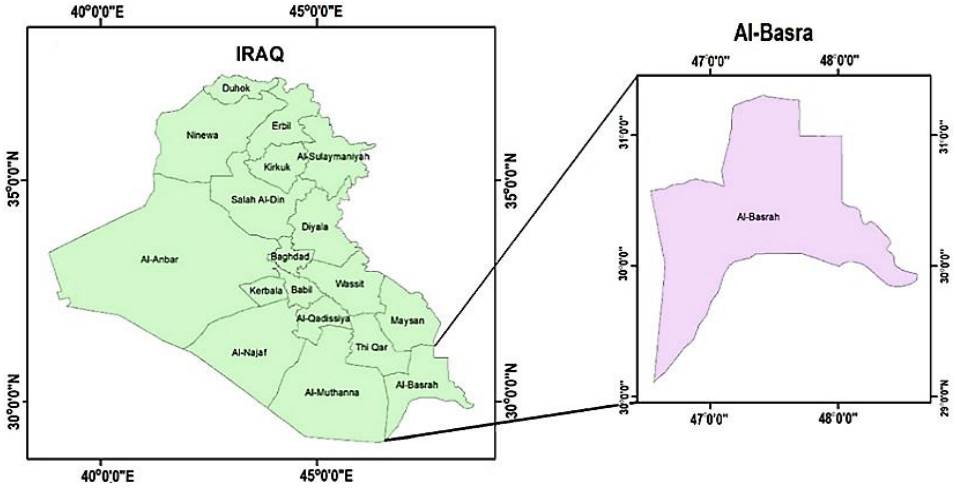

Figure 1. The study area located in South of Iraq, it is one of oil and gas onshore block in Iraq

2.4. Methodology

The method used in the proposed study to evaluate LST is depicted in Figure 2 and it is used to process landsat-8 data that were geometrically corrected. The proposed action steps are explained in detail in the following literature.

- Step-1: the proposed work's first step is to use the following equation to convert digital number (DN) values to top of atmosphere radiance (TOA) for band 10 [12], [17]-[19].

$$L_\lambda = M_L \times Qcal + A_L - O_i \quad (1)$$

Where, Q_{cal} = quantized and calibrated standard product pixel values; L_λ = Top of atmosphere radiance ($Watts / (m2 \times sr \times \mu m)$); A_L = radiance add band 10; M_L = radiance multiplicative band 10; O_i = correction value for band 10

- Step-2: conversion TOA radiance to brightness temperate using thermal constant values in a metadata file and the (2).

$$BT = \frac{K2}{ln\left[\left(\frac{K_1}{L_\lambda}\right)+1\right]} - 273.15 \quad (2)$$

Where, BT = top of atmosphere brightness temperature (°C); K_1 and K_2 are thermal band 10 constants that can be found in the satellite image's metadata file. To convert the temperature from Kelvin to Celsius, the limit must be added (-273.15).

- Step-3: the NDVI is critical for identifying the study area's various land cover types. The NDVI scale runs from -1 to +1. Through The difference between infrared band 5 and red band 4 can be calculated the NDVI of the images using (3).

$$NDVI = \frac{(NIR-RED)}{(NIR+RED)} \quad (3)$$

Where, NDVI = normalized difference vegetation index; NIR = near infra-red band; R = red band.

- Step-4: proportional vegetation refers to estimating the proportion of an area It distinguishes vegetation from land cover by pixels. *Pv* can be calculated using (4).

$$P_v = \left(\frac{NDVI - NDVI_S}{NDVI_v - NDVI_S}\right)^2 \quad (4)$$

Where, NDVIs is the NDVI of soil, NDVIv is the NDVI of vegetation.

- Step-5: the land surface emissivity (LSE) is a proportionality factor that measures the black body radiance to quantify emitted radiance and it is necessary to estimate LST. Furthermore, the LSE is highly affected by surface roughness, vegetation cover, and other factors:

$$E = 0.004 \times Pv + 0.986 \quad (5)$$

Where, *E* = the land surface emissivity and *Pv* = proportion of vegetation.

- Step-6: finally, the LST can be derived depending on the proportional vegetation and emissivity. Using the (6) [20].

$$T_s = \frac{BT}{\left\{1+\left[\left(\frac{\lambda BT}{\rho}\right)\ln \varepsilon_\lambda\right]\right\}} \quad (6)$$

Where, T_s = LST in Celsius (^{o} C);
λ = the wavelength of band 10;
ε_λ = the emissivity; ρ = 1.438x10^{-2} mK

- Step-7 (interpolation): Kriging interpolation is based on statistical models (i.e. including auto-correlation) Geostatistical techniques can produce a forecast surface and also provide accurate forecasts. Kriging supposes that the distance or direction between the measured points reflects spatial correlation to explain the surface variation. The Kriging tool uses a mathematical relationship to determine the resulting values for each site within a given radius [21]. It is a multi-stage process that includes data exploration, analysis, surface creation, variogram modeling, and variance exploration. Kriging is best when you know that the data are spatially correlated or directed. Often it is used in the geology and soil sciences. Kriging is weighs its surrounding values to make a prediction for a non-rated location. Its general equation [22].

$$\hat{Z}(s_0) = \sum_{i=1}^{N} \lambda_i Z(s_i) \quad (7)$$

Where: $Z(s_i)$ = the measured value at the i^{th} location; λ_i = unknown weight for the measured value at the i^{th} location; s_o = the prediction location; N = the number of measured values.

The weight in the ordinary Kriging process depends on the distance between the measured points and the expected location and the spatial relationship between the measured points around the location of the prediction, the parts that follow describe how to make a map of the prediction surface and a map of prediction accuracy using the general Kriging formula. To create a prediction surface map using the Kriging method there are two primary functions:

a) Discover the rules of dependence
b) Create the forecasts

In order to perform these two functions, it is a two-stage process:

a) It produces the covariance and variogram functions to assess the statistical dependency values that are dependent on the sample autocorrelation
b) It forecasts unknown values [23]

Summary the Kriging method uses the data twice:

a) First, an estimate of the spatial relationship between the measured points
b) Second, forecasting unknown values [24]

- Step-8 (gradient): the Image gradient is defined as the directional slope of an image's tonal density and is used frequently for multivariate functions [25]. That incorporates pixel color changes on both the x-axes and y-axes. It is a vector of partial derivatives of all the variables [26]. Supposing that f (*x*, *y*) represents the color of the pixel at (*x*, *y*), the gradient vector of this location. It is defined as (8).

$$\nabla f(x,y) = \begin{bmatrix} g_x \\ g_y \end{bmatrix} = \begin{bmatrix} \partial f/\partial x \\ \partial f/\partial y \end{bmatrix} = \begin{bmatrix} f(x+1,y) - f(x-1,y) \\ f(x,y+1) - f(x,y-1) \end{bmatrix} \quad (8)$$

The partial derivative of an x-axis is represented by the symbol ($\partial f/\partial x$). Measured as $f(x+1,y) - f(x-1,y)$, similarly, the partial derivative of a y-axis is represented by the symbol ($\partial f/\partial y$), measured as $f(x,y+1) - f(x,y-1)$.

There are two important aspects to image gradient [27]:

a) The magnitude is $g = \sqrt{g_x^2 + g_y^2}$

b) The direction is $\theta = \arctan\left(g_y/g_x\right)$

The gradient of an image is a measurement of how it changes. It provides two types of information. The gradient magnitude tells us how fast the image is changing. While the gradient direction tells us the direction in which the image is changing [28]. This vector's length supplies the gradient value. While it gives its direction the gradient direction. Since the gradient can vary at each image location, we use a different vector to represent it [29].

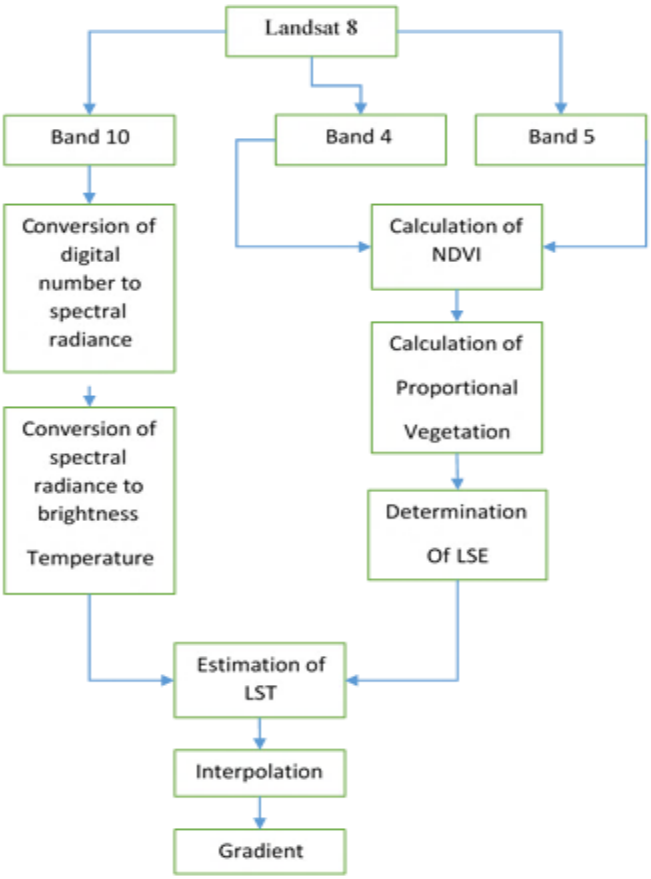

Figure 2. Flow chart diagram

3. RESULTS AND ANALYSIS

The findings revealed that there are 60 thermal anomaly locations in the study area and that the lowest and highest temperature value is 24.2 ºC to 91.11 ºC. Three different sites were chosen in terms of shape, area, and effect. Which is located in the northern and southern Rumaila and Zubair fields, as in Figure 3, Figure 4 and Figure 5.

After identifying the anomalous areas. The spatial distribution of the temperature in the region was obtained by applying the Kriging method (which is one of the geo-statistical interpolation methods. For this reason, interpolation methods are used to getting complete surface information). Spatial interpolation is the process of calculating an unknown value using a group of sample points with known values dispersed throughout a region. The distance between the cell with uncertain value and the sample cells adds to the estimate of its ultimate value. The objective of spatial interpolation is to generate a surface that best represents the sampled event. The first site's interpretation of interpolation techniques was displayed. The shape is semi-oval, with the darker blue color in the center representing the maximum temperature value,

and the further away from the middle the color tends to light because the temperature gradually decreases. It is one source of hydrocarbon seepage, and it represents the well, which appears in dark blue, and the light blue color indicates the spread of hydrocarbons around it. As in Figure 6, while at the second site there are two hydrocarbon seepage close together, one strong appears dark blue and the other is weak, as in Figure 7. Finally, the third site shows more than one source of hydrocarbon seepage spreading over a wide distance. It also appears in Figure 8 in dark blue. A gradient determination method has been applied to get more information about its location, extension, size, shape, and trends. It also appears in Figure 9, Figure 10, and Figure 11 where the direction of the arrow indicates areas of leakage. The result of gradient and interpolation methods was effective to detect evidence of hydrocarbon estimate significant areas that have hydrocarbon seepage in the study area which may be promising for exploration and production of oil and gas.

Figure 3. Image Google Earth view location of hydrocarbon seepage for Southern Rumaila oil field in the anomalous area-1

Figure 4. Image Google Earth view location of hydrocarbon seepage for Zubair oil field in the anomalous area-2

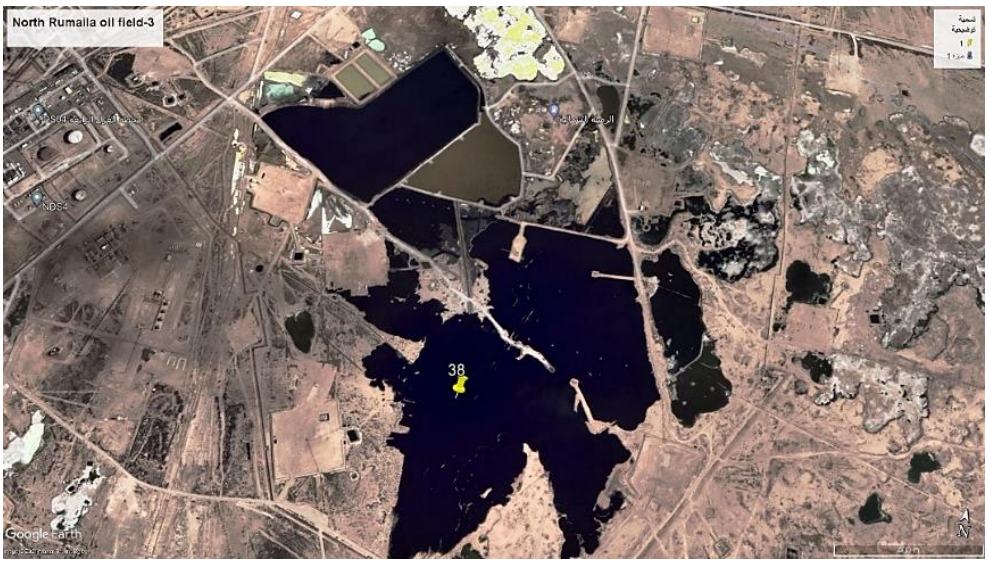

Figure 5. Image Google Earth view location of hydrocarbon seepage for Northern Rumaila oil field in the anomalous area-3

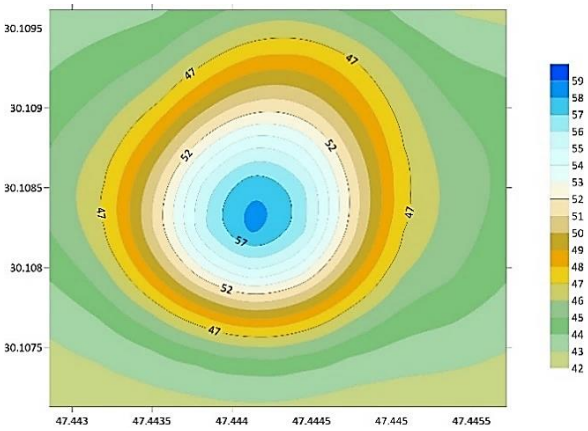

Figure 6. Interpolation of area-1 using Kriging method

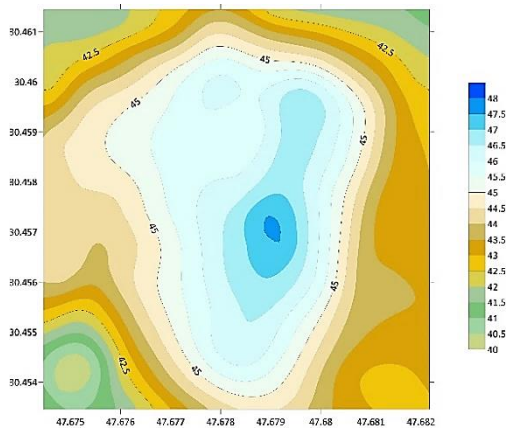

Figure 7. Interpolation of the H.C distribution for area-2 using Kriging method

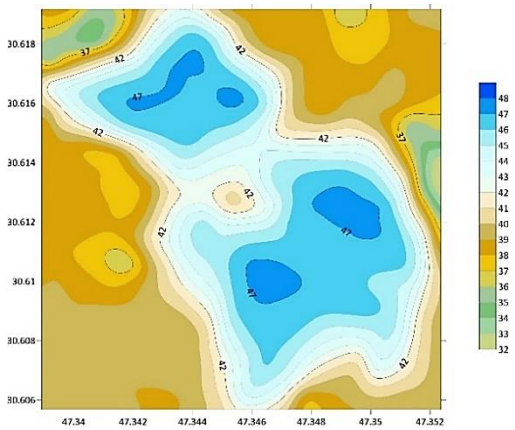

Figure 8. Interpolation of the H.C distribution for area-3 using Kriging method

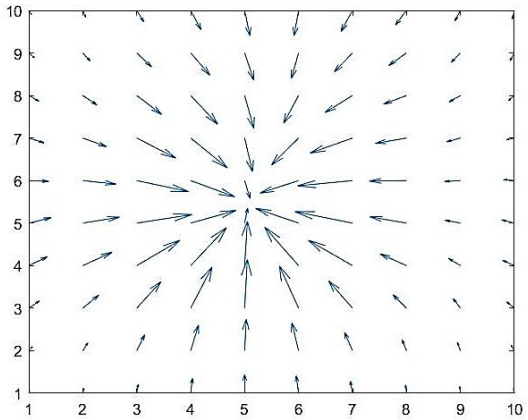

Figure 9. The gradient map for Southern Rumaila oil

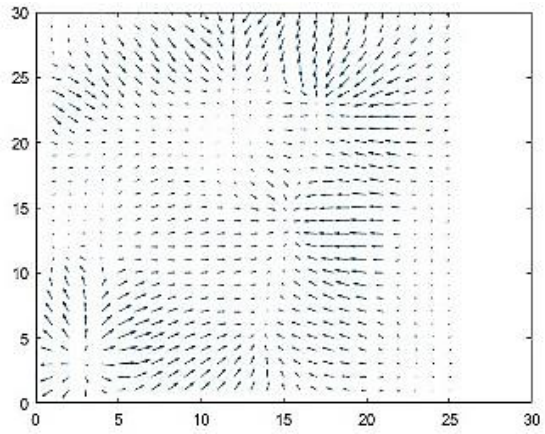

Figure 10. The gradient map for Zubiar oil field

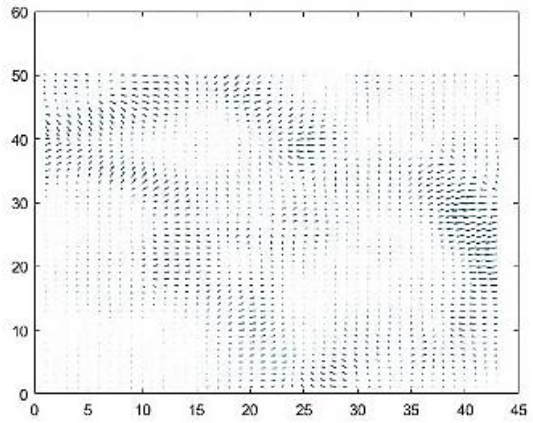

Figure 11. The gradient map for Northern Rumaila oil field

4. CONCLUSION

This paper presents a new method for determining the locations of hydrocarbon leaks on the surface using the temperature data obtained from the landsat-8 satellite images to determine the extent of the oil spill statistically by using spatial interpolation and gradient techniques. This study illustrates that landsat-8 TIR can be used for the exploration of gas and oil resources by HC micro seepage detection in the region. The detection of gas and oil resources is conducted by temperature data. The findings of this study show that the HC micro-seepage range spreads in the region around the oil field. The results showed high accuracy in determining the locations of oil spills and the size of them after identifying the anomalies areas The results achieved were very rational and showed high accuracy in determining the source of the leak when compared to Google Earth images, and we note the presence of a flame at the site of the leak. The proposed approach in this study would help determine the shape of the anomaly and reveal the spatial relationships between the mapped anomaly and possible subsurface.

REFERENCES

[1] M. I. J. Putra, D. N. Huda, F. Afdhalia, and Supriatna, "Onshore oil and gas reservoir detection through mapping of hydrocarbon microseepage using remote sensing," *IOP conference Series Earth and Environmental Science*, vol. 311, no. 1, Aug. 2019, doi: 10.1088/1755-1315/311/1/012083.

[2] S. Asadzadeh and C. R. d. S. Filho, "Spectral remote sensing for onshore seepage characterization: A critical overview," *Earth-Science Reviews*, vol. 168, pp. 48-72, May 2017, doi: 10.1016/j.earscirev.2017.03.004.

[3] M. N. Jha, J. Levy, and Y. Gao, "Advances in remote sensing for oil spill disaster management: State-of-the-art sensors technology for oil spill surveillance," *Sensors*, vol. 8, no. 1, pp. 236–255, Jan. 2008, doi: 10.3390/s8010236.

[4] M. Fingas and C. Brown, "Review of oil spill remote sensing," *Marine Pollution Bulletin*, vol. 83, no. 1. pp. 9-23, 2014, doi: 10.1016/j.marpolbul.2014.03.059.

[5] G. Zhang, L. Zou, X. Shen, S. Lu, C. Li, and H. Chen, "Remote sensing detection of heavy oil through spectral enhancement techniques in the western slope zone of Songliao Basin, China," *American Association of Petroleum Geologists Bulletin*, vol. 93, no. 1, pp. 31-49, 2009, doi: 10.1306/08110808002.

[6] D. Dubucq and A. Ebner, "Remote sensing onshore hydrocarbon direct detection for exploration: why is it different?," *Proc. SPIE 11156, Earth Resources and Environmental Remote Sensing/GIS Applications X 111560P*, 2019, vol. 11156, doi: 10.1117/12.2533192.

[7] H. Shen, P. Zhou, and, S. Feng, "Research on multi-angle near infrared spectral-polarimetric characteristic for polluted water by spilled oil," *Proc. SPIE 8193, International Symposium on Photoelectronic Detection and Imaging 2011: Advances in Infrared Imaging and Applications, 81930M*, 2011, vol. 8193, doi: 10.1117/12.899035.

[8] M. Fingas and C. Brown, "Oil Spill Remote Sensing," in *Encyclopedia of Sustainability Science and Technology*, New York, NY: Springer New York, 2012, pp. 7491-7527, doi:10.1007/978-1-4419-0851-3_732.

[9] C. Mätzler, *Thermal Microwave Radiation: Applications for Remote Sensing*. pp. 1-556, 2006, doi: 10.1049/PBEW052E.

[10] R. P. Gupta, *Remote Sensing Geology*: *Third Edition*. pp. 1-428, 2017, doi: 10.1007/978-3-662-55876-8.

[11] M. S. Ozigis, J. D. Kaduk, and C. H. Jarvis, "Mapping terrestrial oil spill impact using machine learning random forest and Landsat 8 OLI imagery: a case site within the Niger Delta region of Nigeria," *Environmental Science and Pollution Research*, vol. 26, no. 4, pp. 3621-3635, Dec 2018, doi: 10.1007/s11356-018-3824-y.

[12] F. Wang, Z. Qin, C. Song, L. Tu, A. Karnieli, and S. Zhao, "An improved mono-window algorithm for land surface temperature retrieval from landsat 8 thermal infrared sensor data," *Remote Sensing*, vol. 7, no. 4, 2015, doi: 10.3390/rs70404268.

[13] X. Yu, X. Guo, and Z. Wu, "Land surface temperature retrieval from landsat 8 TIRS-comparison between radiative transfer equation-based method, split window algorithm and single channel method," *Remote Sensing*, vol. 6, no. 10, 2014, doi: 10.3390/rs6109829.

[14] M. Fingas and C. E. Brown, "A review of oil spill remote sensing," *Sensors*, vol. 18, no. 1, pp. 1-18, 2018, doi: 10.3390/s18010091.

[15] W. Alpers, B. Holt, and K. Zeng, "Oil spill detection by imaging radars: Challenges and pitfalls," *Remote Sensing Environment*, vol. 201, pp. 133-147, Nov. 2017, doi: 10.1016/j.rse.2017.09.002.
[16] R. Al-Ruzouq *et al*., "Sensors, features, and machine learning for oil spill detection and monitoring: A review," *Remote Sensing*, vol. 12, no. 20, 2020, doi: 10.3390/rs12203338.
[17] D. Jeevalakshmi, S. N. Reddy, and B. Manikiam, "Land cover classification based on NDVI using LANDSAT8 time series: A case study Tirupati region," *2016 International Conference on Communication and Signal Processing (ICCSP)*, 2016, pp. 1332-1335, doi: 10.1109/ICCSP.2016.7754369.
[18] R. Zhibin, Z. Haifeng, H. Xingyuan, Z. Dan, and Y. Xingyang, "Estimation of the Relationship Between Urban Vegetation Configuration and Land Surface Temperature with Remote Sensing," *Journal of the Indian Society of Remote Sensing*, vol. 43, no. 1, pp. 89-100, 2015, doi: 10.1007/s12524-014-0373-9.
[19] J. A. Barsi, J. R. Schott, S. J. Hook, N. G. Raqueno, B. L. Markham, and R. G. Radocinski, "Landsat-8 thermal infrared sensor (TIRS) vicarious radiometric calibration," *Remote Sensing*, vol. 6, no. 11, 2014, doi: 10.3390/rs61111607.
[20] Yuhendra and J. T. S. Sumantyo, "Assessment of Landsat 8 TIRS data capability for the preliminary study of geothermal energy resources in West Sumatra," *TELKOMNIKA Telecommunication Computing Electronics and Control*, vol. 18, no. 5, pp. 2737–2747, 2020, doi: 10.12928/TELKOMNIKA.v18i5.16172.
[21] Y. Xie *et al*., "Spatial distribution of soil heavy metal pollution estimated by different interpolation methods: Accuracy and uncertainty analysis," *Chemosphere*, vol. 82, no. 3, pp. 468-476, Jan. 2011, doi: 10.1016/j.chemosphere.2010.09.053.
[22] D. Ozturk and F. Kilic, "Geostatistical approach for spatial interpolation of meteorological data," *Anais da Academia Brasileira de Ciências*, vol. 88, no. 4, pp. 2121-2136, Oct. 2016, doi: 10.1590/0001-3765201620150103.
[23] J. Li and A. D. Heap, "A Review of Spatial Interpolation Methods for Environmental Scientists," *Geoscience Australia Record 2008/23*, p. 154, 2008. [Online]. Available: https://data.gov.au/data/dataset/a-review-of-spatial-interpolation-methods-for-environmental-scientists/resource/a3eb8947-ad4f-49b7-97b1-1363df4be902.
[24] B. Schneider and D. Martinoni, "A distributed geoprocessing concept for enhancing terrain analysis for enviromental modeling," *Transactions in GIS*, vol. 5, no. 2, pp. 165-178, 2001, doi: 10.1111/1467-9671.00074.
[25] G. Tzimiropoulos, S. Zafeiriou and M. Pantic, "Subspace Learning from Image Gradient Orientations," in *IEEE Transactions on Pattern Analysis and Machine Intelligence*, vol. 34, no. 12, pp. 2454-2466, Dec. 2012, doi: 10.1109/TPAMI.2012.40.
[26] T. S. Cho, C. L. Zitnick, N. Joshi, S. B. Kang, R. Szeliski, and W. T. Freeman, "Image Restoration by Matching Gradient Distributions," in *IEEE Transactions on Pattern Analysis and Machine Intelligence*, vol. 34, no. 4, pp. 683-694, April 2012, doi: 10.1109/TPAMI.2011.166.
[27] R. C. Gonzalez and R. E. Woods, *Digital Image Processing (3rd Edition)*, 2007, pp. 976. [Online]. Available: http://sdeuoc.ac.in/sites/default/files/sde_videos/Digital%20Image%20Processing%203rd%20ed.%20-%20R.%20Gonzalez%2C%20R.%20Woods-ilovepdf-compressed.pdf
[28] M. Sadowski and A. Grzegorczyk, "Image Inpainting with Gradient Attention," *Schedae Informaticae*, vol. 27, pp. 81-91, 2018, doi: 10.4467/20838476SI.18.007.10412.
[29] L. Shapiro and G. Stockman, *Computer Vision 1st Edition*, 2001, pp. 608. [Online]. Available: http://nana.lecturer.pens.ac.id/index_files/referensi/computer_vision/Computer%20Vision.pdf

BIOGRAPHIES OF AUTHORS

Dheya Uldeen K. Abbas was born in Baghdad, Iraq, in 1996. He received the bachelor degree in physics, Baghdad in 2017, and currently working towards a master's degree at the University of Baghdad, Iraq. His current research interest includes; artificial intelligence, image processing, GIS, remote sensing. He can be contacted at email: dhiaa.khdeer1204@sc.uobaghdad.edu.iq.

Loay E. George is Assistant Professor, Ph. D holder since 1979, I was a member of teaching staff in college of science/ Baghdad University, Iraq. Currently working as assistant of UoITc President for Scientific Affairs. My main research concerns are: digital multimedia processing, coding (encryption, digital signature, data compression, and representation), pattern recognition & classification, fast strings processing and analysis, biometrics, and visual based application. He can be contacted at email: loayedwar57@yahoo.com.